ChemComm

COMMUNICATION

View Article Online
View Journal | View Issue

Cite this: *Chem. Commun.*, 2018, **54**, 12646

Received 15th August 2018,
Accepted 12th October 2018

DOI: 10.1039/c8cc06652c

rsc.li/chemcomm

Tetrahedral metal–organic cages with cube-like cavities for selective encapsulation of fullerene guests and their spin-crossover properties†

Wang-Kang Han,[a] Hai-Xia Zhang,[a] Yong Wang,[b] Wei Liu,[b] Xiaodong Yan,[a] Tao Li[a] and Zhi-Guo Gu*[ac]

Tetrahedral $Fe^{II}_4L_6$ coordination cages containing organic linkers with rigid π-electron aromatic rings and flexible alkyl units were constructed. Interestingly, these tetrahedral cages have rare cube-like cavities for selective encapsulation of fullerene guests. In addition, the solid state spin-crossover properties were influenced by guest binding of fullerene C_{60}.

Considerable attention has been paid to the construction of container molecules in recent years for their wide ranging applications in separation,[1] recognition,[2] catalysis,[3] gas storage,[4] stabilization of reactive species[5] and so on.[6] Metal–organic cages (or coordination cages) with porous surfaces and abundant recognition sites in their central cavities can typically bind guest molecules through specific host–guest interactions and molecular recognition.[7,8] The design and modulation of the size and shape of the cage cavity to selectively accommodate guest molecules, fullerenes for example, is still an enormous challenge due to their similar physicochemical properties. To date, research on metal–organic cages for the separation and purification of fullerene guests has been mainly focused on those cages with rigid ligands.[9,10] However, the composition and structure of rigid ligands are quite limited; moreover, the rigid coordination cages always lack flexibility and selectivity for encapsulation of different fullerene guests. Therefore, the design of metal–organic cages with enough flexibility to accommodate fullerene guests is important.

To develop metal–organic cages capable of selective encapsulation of fullerene guests, three main factors need to be considered: (i) the cavity shape and size of the cages should be suitable for capturing target fullerene guests; (ii) the inner voids should be surrounded by π-electron-rich ligands, which could enhance the affinity towards spherical fullerene guests through aromatic stacking interactions; (iii) the window of the cage should be flexible enough to allow guests to enter and exit the host for isolating guests from the environment. In order to construct the target metal–organic cages, the ligands should combine with rigid π-electron groups and flexible linkers (Scheme 1). With this in mind, we incorporated O–benzene or O–naphthalene moieties and flexible alkyl units into the ligands. The O–benzene or O–naphthalene moieties could provide favorable binding sites for the fullerene guest through aromatic stacking and donor–accepter interactions, while the alkyl chains on both sides of the aromatic panels were expected to enhance the flexibility of the ligands.

Employing these strategies, rigid-flexible di(imidazole aldehyde) components, (*R*)-1-(naphthalen-2-yl)ethanamine and iron(II) ions, were chosen as the building blocks for the construction of metal–organic cages through a multicomponent self-assembly process (Fig. 1). Herein, we described the design, syntheses, crystal structures and host–guest behaviors of flexible $Fe^{II}_4L_6$ (L = 1,2-di((imidazol-2-ylmethylene)-(*R*)-1-phenylethanamine)ethane derivatives) tetrahedral metal–organic cages. The coordination cages presented rare

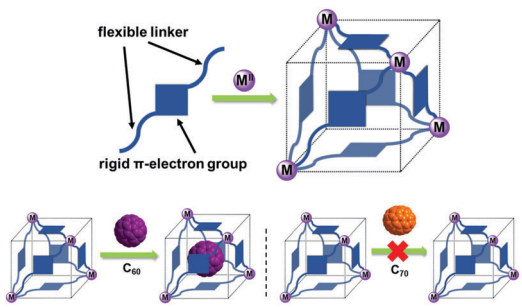

Scheme 1 Schematic representation of the building blocks used for the design of metal–organic cages with selective encapsulation of fullerene guests.

[a] The Key Laboratory of Synthetic and Biological Colloids, Ministry of Education, School of Chemical and Material Engineering, Jiangnan University, Wuxi 214122, P. R. China. E-mail: zhiguogu@jiangnan.edu.cn
[b] College of Chemistry, Chemical Engineering and Material Science, Soochow University, Su Zhou 215123, P. R. China
[c] International Joint Research Center for Photoresponsive Molecules and Materials, School of Chemical and Material Engineering, Jiangnan University, Wuxi 214122, P. R. China

† Electronic supplementary information (ESI) available: Experimental details, general characterizations, additional plot and discussion. CCDC 1847958 and 1847959. For ESI and crystallographic data in CIF or other electronic format see DOI: 10.1039/c8cc06652c

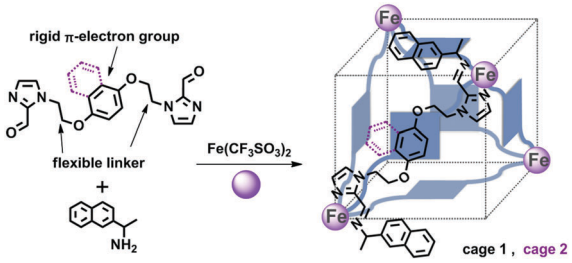

Fig. 1 Design and synthesis of tetrahedral metal–organic cages **1** and **2** with cube-like cavities through a multicomponent self-assembly approach.

cube-like cavities, and displayed selective encapsulation of fullerene guests. In addition, the solid state spin-crossover behaviors and the influence of the fullerene guest on the magnetic properties of the two types of $Fe_4^{II}L_6$ coordination cages were also investigated.

The self-assembly reactions of the di(imidazole aldehyde) components (6 equiv.), iron(II) trifluoromethanesulfonate ($Fe(OTf)_2$, 4 equiv.) and (*R*)-1-(naphthalen-2-yl)ethanamine (12 equiv.), in acetonitrile solution resulted in the formation of tetrahedral $Fe_4^{II}L_6$ cages **1** and **2** (see the ESI†). The microstructures of cages **1** and **2** were characterized by FT-IR, UV-vis, NMR spectroscopy, mass spectroscopy, and single crystal X-ray diffraction analysis. FT-IR spectra of cages **1** and **2** showed strong absorption in the region around 1573–1601 cm^{-1}, which was typical for stretching of imidazole-imine (C=N) groups. The peaks at about 1258 cm^{-1} and 636 cm^{-1} revealed the existence of OTf^- anions in the metal–organic cage complexes (Fig. S9, ESI†). High-resolution mass spectra (HRMS) showed ion peaks at m/z = 2541.18, 1644.47 and 1196.12 (Fig. S22–S25, ESI†), corresponding to $[\mathbf{1}(OTf)_6]^{2+}$, $[\mathbf{1}(OTf)_5]^{3+}$ and $[\mathbf{1}(OTf)_4]^{4+}$, respectively, while the ion peaks observed at m/z = 2691.24, 1744.50 and 1271.14 (Fig. S26–S29, ESI†) correspond very well to $[\mathbf{2}(OTf)_6]^{2+}$, $[\mathbf{2}(OTf)_5]^{3+}$ and $[\mathbf{2}(OTf)_4]^{4+}$, respectively. The observed ion peaks agreed well with the simulated isotopic patterns, further verifying the formation of a Fe_4L_6 stoichiometry of cages **1** and **2**.

Single crystal X-ray diffraction analysis at 173 K confirmed the edge-capped capsule structures of the $[Fe_4L_6]^{8+}$ for cages **1** and **2**. As shown in Fig. 2, each iron(II) centre coordinated with six nitrogen atoms from three imidazole-imine Schiff-base type ligands, forming a distorted octahedral FeN_6 coordination geometry, and the four Fe(II) metal nodes were bridged by six ligand linkers, forming a tetrahedral cage with approximate *T* point symmetry. The metal centres occupied the vertices and the linkers situated at the edges of the tetrahedron. All metal centres displayed facial coordination and share the same *Λ* handedness. The average Fe–N bond length of cage **1** was 1.96 Å, and the average Fe–N bond length of cage **2** was slightly longer at 1.98 Å. These values were consistent with the typical low-spin iron(II) centres at 173 K.[11] The metal–metal spacing was in the range of 11.588–12.846 Å for cage **1**, and 12.052–12.351 Å for cage **2**. In each $[Fe_4L_6]^{8+}$ cation, twelve intramolecular face-to-face π–π stacking interactions existed between each parallel naphthalene ring and imidazole ring of the adjacent ligands, further stabilizing the supramolecular structure (Fig. S30–S31, ESI†).

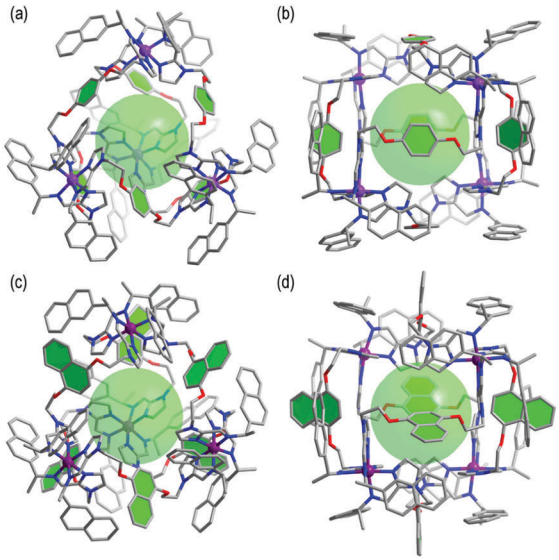

Fig. 2 Two views of the cationic parts of the X-ray crystal structures: (a) and (b) for cage **1**; (c) and (d) for cage **2**. All H atoms, counter anions, solvent molecules and disorder have been omitted for clarity (C, grey; N, blue; O, red; Fe, purple).

The average center-to-center distance of the π–π stacking was 3.88 Å for cage **1** and 3.72 Å for cage **2**.

Interestingly, unlike the reported edge-capped M_4L_6 coordination cages with rigid linkers and tetrahedral cavities, cages **1** and **2** possessed rare cube-like cavities due to the flexible alkyl chains such that the linkers could be rotated and distorted. As a result, six O–benzene (or O–naphthalene) moieties are situated at each face, and four iron(II) ions occupied half of the vertices of the artificial cube. For cage **1**, four O–benzene moieties are parallel to the cube face in a "face to face" state, while another two O–benzene moieties are vertical to the cube face in an "edge to edge" state (Fig. S32, ESI†). For cage **2**, all the O–naphthalene moieties are vertical to the artificial cube face in an almost "edge to edge" state (Fig. S33, ESI†). The resulting cube-like cavities in cages **1** and **2** surrounded with O–benzene or O–naphthalene moieties could provide favorable binding sites for aromatic guest molecules through π–π stacking interactions and donor–acceptor interactions. In addition, the windows of cages **1** and **2** were opened with large pores to allow the guests to enter and exit (Fig. 2). The cavity volumes were calculated to be 608 and 563 $Å^3$ for cages **1** and **2**, respectively. The large cube-like void volume with π-electron density revealed by single crystal structural analysis stimulated us to explore the capability of cages **1** and **2** to act as receptors for fullerene guests. NMR spectroscopy and high-resolution mass spectrometry characterizations were thus carried out to investigate their encapsulation of fullerene guests.

Upon addition of C_{60} guests to cage **1** or cage **2** in CD_3CN, the signals on the ^{1}H-NMR spectra displayed a significant chemical shift, especially the aromatic C–H signals between 5.2 ppm and 8.5 ppm (Fig. 3). After equilibrating the mixture of cage **1** and fullerene C_{60} at 50 °C for 24 h, a new set of ^{1}H-NMR single peaks was observed at different chemical shifts while the

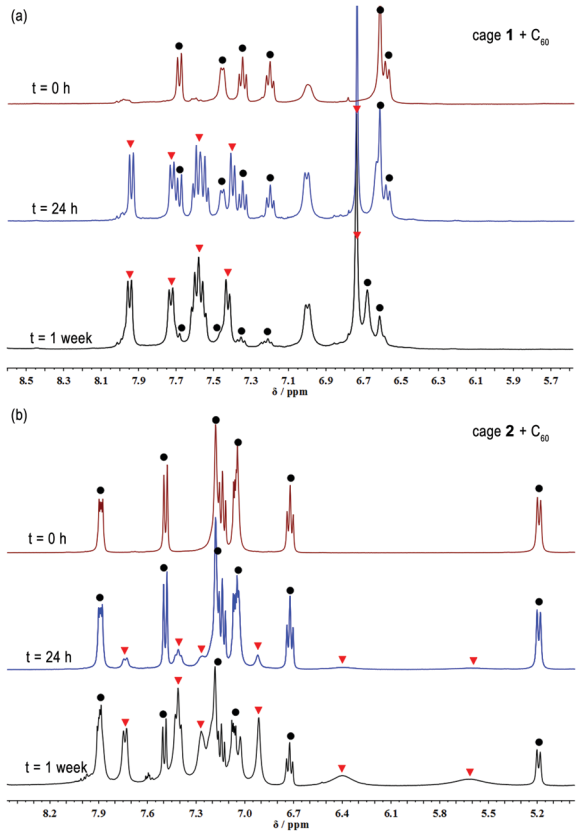

Fig. 3 Partial ^{1}H-NMR spectra (400 Hz, CD_3CN, 298 K) of (a) a mixture of cage **1** and C_{60} (about 5 equiv.) and (b) a mixture of cage **2** and C_{60} (about 5 equiv.), allowed to equilibrate at 50 °C for 0 h, 24 h and one week.

peaks corresponding to the empty host had partially disappeared, which could be attributed to the formation of [$C_{60}\subset$**1**] host–guest complexes.[12] Further equilibrating the mixture for one week, nearly all the peaks corresponding to the empty cage disappeared, indicating that most of the cages were converted to the host–guest complexes (Fig. 3a). Similar trends in the ^{1}H-NMR spectra were also observed after equilibrating the mixture of cage **2** and C_{60}, as evidenced by the disappearance of the peaks corresponding to the free host and concurrent appearance of a new set of peaks corresponding to the host–guest complex [$C_{60}\subset$**2**]. However, even after the mixture of cage **2** and C_{60} was allowed to equilibrate at 50 °C for one week, the ^{1}H-NMR signals from the empty cage **2** and host–guest complexes [$C_{60}\subset$**2**] still coexisted (Fig. 3b). This observation indicated that cage **1** had a better preference to C_{60} than cage **2**. We proposed that C_{60} was bound more strongly within cage **1** than in cage **2**, possibly due to a better match in terms of size and shape and thus the stronger π–π interactions. In addition, new NMR signals and chemical shifts were also detected in the ^{13}C-NMR spectra after equilibrating the mixture of cage hosts and C_{60} guests (Fig. S34, S35, S38 and S39, ESI†). It was worth noting that the ^{13}C-NMR spectra showed an intense peak at 142 ppm from C_{60} despite the negligible solubility of C_{60} in CD_3CN, which further provided evidence for the encapsulation of C_{60} by the host cages **1** and **2** (Fig. S34 and S38, ESI†).[9b,13]

Nevertheless, no C_{70} encapsulation in the cage **1** or **2** was detected, as indicated by the ^{1}H NMR spectra of the hosts which appeared nearly at the same chemical shifts as in the absence of the C_{70} guest (Fig. S42 and S43, ESI†).

Furthermore, the formation of 1 : 1 host–guest complexes, [$C_{60}\subset$**1**] and [$C_{60}\subset$**2**], was also supported by the HRMS analysis. The former exhibited intense signal peaks which corresponded to three different species: $[C_{60}\subset\mathbf{1}(OTf)_5]^{3+}$, $[C_{60}\subset\mathbf{1}(OTf)_4]^{4+}$, and $[C_{60}\subset\mathbf{1}(OTf)_3]^{5+}$ at m/z = 1884.47, 1376.13, and 1071.10 (Fig. 4a), respectively. The latter, [$C_{60}\subset$**2**], gave ion peaks at m/z = 1984.83, 1451.40, and 1131.12 corresponding to the $[C_{60}\subset\mathbf{2}(OTf)_5]^{3+}$, $[C_{60}\subset\mathbf{2}(OTf)_4]^{4+}$, and $[C_{60}\subset\mathbf{2}(OTf)_3]^{5+}$ charge states, respectively (Fig. 4b). Besides, the isotopic distributions of the experimental results were also well consistent with the simulated isotopic patterns (Fig. S44–S51, ESI†).

We inferred from the significant differences of the guest binding results, that the smaller C_{60} proved to be a better guest than C_{70}, could be rationalized by comparing the size and shape match between the host cavities and the fullerene guests. The van der Waals volume of C_{60} is 345 Å^3, taking up 56.74% of the cavity of cage **1**, while the van der Waals volume of C_{70} is 390 Å^3, occupying 64.14% of the cavity of cage **1**.[14] On the other hand, the volumes of C_{60} and C_{70} are about 61.28% and 67.27% of the cavity of cage **2**, respectively. According to Julius Rebek's 55% rule, which is based on the volume ratio of the guest and the host,[15] it is thus obvious that the cavities of cages **1** and **2** are good match for C_{60}, and that both cages **1** and **2** are not suitable for C_{70}. For cages **1** and **2**, the C_{60} guest was closer to the optimum occupation in favor of forming host–guest complexes, while the C_{70} guest was too large to situate in the host cavities. Therefore, cages **1** and **2** were expected to show good performance for selective encapsulation of C_{60} and C_{70} guests.

Magnetic interaction and guest dependent spin-crossover (SCO) properties in multinuclear SCO compounds have aroused particular interest. And magnetic susceptibilities for cages **1** and **2** were determined. Both cages **1** and **2** exhibited typical gradual and incomplete SCO behaviors. As shown in Fig. 5, the $\chi_M T$ values of cages **1** and **2** remain almost constant (about 1.64 cm^3 K mol^{-1} for cage **1** and 1.55 cm^3 K mol^{-1} for cage **2**) below 200 K, suggesting that most of the Fe(II) centers were in the low-spin state at low temperatures. Upon further heating, the $\chi_M T$ value gradually increased and reached its maximum

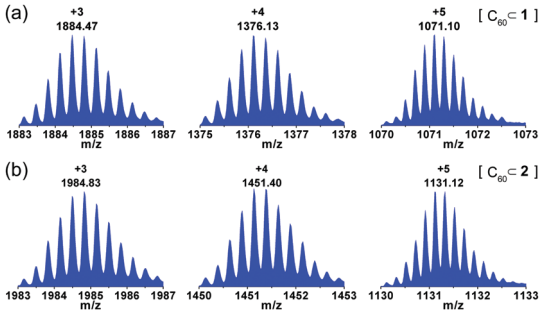

Fig. 4 High-resolution mass spectra of (a) [$C_{60}\subset$**1**] and (b) [$C_{60}\subset$**2**] showing the +3, +4 and +5 ion peaks.

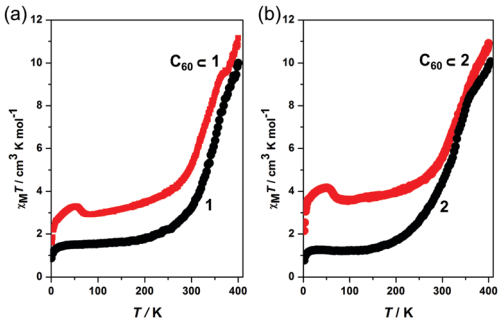

Fig. 5 Variable-temperature solid-state magnetic susceptibility measurements for (a) cage **1** and [$C_{60}\subset$**1**], (b) cage **2** and [$C_{60}\subset$**2**].

value of 9.95 cm^3 K mol^{-1} for cage **1** and 8.83 cm^3 K mol^{-1} for cage **2** at 400 K. The spin-transition temperature $T_{1/2}$ was estimated to be 344 K for cage **1** and 328 K for cage **2**. The ^{1}H chemical shift values of the signals attributed to cages **1** and **2** were also observed to increase with temperature (Fig. S59 and S60, ESI†). The imine peak showed the largest increase due to its proximity to the metal center. This shift was consistent with an increase in the high-spin population of iron(II) ions.

Spin-crossover behaviors were also observed in the host–guest complexes [$C_{60}\subset$**1**] and [$C_{60}\subset$**2**]. However, there are two major differences: firstly, the inclusion of the C_{60} guest resulted in stabilization of the high-spin state of iron(II) centers, since $T_{1/2}$ was lowered by approximately 32 K for [$C_{60}\subset$**1**] (estimated $T_{1/2}$ = 312 K) and 22 K for [$C_{60}\subset$**2**] (estimated $T_{1/2}$ = 306 K). This may be due to the SCO-active hosts accommodating the fullerene guest by changing their geometry to a greater extent than for the empty hosts, leading to an increase in the high-spin population at the same temperatures.[16] Secondly, as the temperature increased from 2 K to 100 K, the $\chi_M T$ showed an abrupt increase up to a maximum value of 3.30 cm^3 K mol^{-1} at 52 K for cage **1** and 4.16 cm^3 K mol^{-1} at 49 K for cage **2**, then decreased to 2.92 cm^3 K mol^{-1} at 80 K for cage **1** and 3.57 cm^3 K mol^{-1} for cage **2** at 89 K. The obvious anomaly in the $\chi_M T$ plots at low temperature may be due to the ferromagnetic transitions resulting from the donor–accepter interactions between the C_{60} guest and Fe(II) ions, and the exchange interaction between π-electrons on C_{60} guest molecules and O–benzene (or O–naphthalene) aromatic ligands.[17]

In conclusion, two iron(II) tetrahedral metal–organic cages with cube-like cavities have been constructed. The two types of iron(II) coordination cages are both capable of selectively encapsulating C_{60} fullerene guests and showing solid state spin-crossover behaviors. Varying the nature of O–benzene or O–naphthalene moieties and changing the alkyl chain linking length may further affect the recognition and selectivity toward various fullerene guests. Moreover, these kinds of metal–organic cages are homochiral, and efforts are currently being pursued for chiral guest discrimination and separation.

This work was supported by the National Natural Science Foundation of China (21771089), the Fundamental Research Funds for the Central Universities (JUSRP51725B and JUSRP51513), the Project for Jiangsu Scientific and Technological Innovation Team, and the MOE & SAFEA for the 111 Project (B13025).

Conflicts of interest

There are no conflicts to declare.

Notes and references

1 (*a*) J. Navarro-Sanchez, A. I. Argente-Garcia, Y. Moliner-Martinez, D. Roca-Sanjuan, D. Antypov, P. Campins-Falco, M. J. Rosseinsky and C. Marti-Gastaldo, *J. Am. Chem. Soc.*, 2017, **139**, 4294–4297; (*b*) K. Wu, K. Li, Y. J. Hou, M. Pan, L. Y. Zhang, L. Chen and C. Y. Su, *Nat. Commun.*, 2016, **7**, 10487; (*c*) T. Liu, Y. Liu, W. Xuan and Y. Cui, *Angew. Chem., Int. Ed.*, 2010, **49**, 4121–4124.
2 (*a*) S. Loffler, A. Wuttke, B. Zhang, J. J. Holstein, R. A. Mata and G. H. Clever, *Chem. Commun.*, 2017, **53**, 11933–11936; (*b*) X. Jing, Y. Yang, C. He, Z. Chang, J. N. H. Reek and C. Duan, *Angew. Chem., Int. Ed.*, 2017, **56**, 11759–11763; (*c*) A. M. Castilla, T. K. Ronson and J. R. Nitschke, *J. Am. Chem. Soc.*, 2016, **138**, 2342–2351.
3 (*a*) L. Zhao, X. Jing, X. Li, X. Guo, L. Zeng, C. He and C. Duan, *Coord. Chem. Rev.*, 2017, DOI: 10.1016/j.ccr.2017.11.005; (*b*) C. Tan, J. Jiao, Z. Li, Y. Liu, X. Han and Y. Cui, *Angew. Chem., Int. Ed.*, 2018, **57**, 2085–2090; (*c*) V. Marti-Centelles, A. L. Lawrence and P. J. Lusby, *J. Am. Chem. Soc.*, 2018, **140**, 2862–2868.
4 (*a*) L. Zhang, L. Xiang, C. Hang, W. Liu, W. Huang and Y. Pan, *Angew. Chem., Int. Ed.*, 2017, **56**, 7787–7791; (*b*) J. S. Wright, A. J. Metherell, W. M. Cullen, J. R. Piper, R. Dawson and M. D. Ward, *Chem. Commun.*, 2017, **53**, 4398–4401.
5 (*a*) D. Yang, J. Zhao, L. Yu, X. Lin, W. Zhang, H. Ma, A. Gogoll, Z. Zhang, Y. Wang, X. J. Yang and B. Wu, *J. Am. Chem. Soc.*, 2017, **139**, 5946–5951; (*b*) P. Mal, B. Breiner, K. Rissanen and J. R. Nitschke, *Science*, 2009, **324**, 1697–1699.
6 (*a*) W. Wang, Y. X. Wang and H. B. Yang, *Chem. Soc. Rev.*, 2016, **45**, 2656–2693; (*b*) L. Yang, X. Jing, B. An, C. He, Y. Yang and C. Duan, *Chem. Sci.*, 2018, **9**, 1050–1057; (*c*) N. Struch, C. Bannwarth, T. K. Ronson, Y. Lorenz, B. Mienert, N. Wagner, M. Engeser, E. Bill, R. Puttreddy, K. Rissanen, J. Beck, S. Grimme, J. R. Nitschke and A. Lützen, *Angew. Chem., Int. Ed.*, 2017, **56**, 4930–4935.
7 (*a*) S. Zarra, D. M. Wood, D. A. Roberts and J. R. Nitschke, *Chem. Soc. Rev.*, 2015, **44**, 419–432; (*b*) N. Ahmad, H. A. Younus, A. H. Chughtai and F. Verpoort, *Chem. Soc. Rev.*, 2015, **44**, 9–25.
8 (*a*) W. Q. Xu, Y. Z. Fan, H. P. Wang, J. Teng, Y. H. Li, C. X. Chen, D. Fenske, J. J. Jiang and C. Y. Su, *Chem. – Eur. J.*, 2017, **23**, 3542–3547; (*b*) J. Guo, Y. W. Xu, K. Li, L. M. Xiao, S. Chen, K. Wu, X. D. Chen, Y. Z. Fan, J. M. Liu and C. Y. Su, *Angew. Chem., Int. Ed.*, 2017, **56**, 3852–3856; (*c*) D. Luo, X. P. Zhou and D. Li, *Angew. Chem., Int. Ed.*, 2015, **54**, 6190–6195.
9 (*a*) W. Brenner, T. K. Ronson and J. R. Nitschke, *J. Am. Chem. Soc.*, 2016, **139**, 75–78; (*b*) T. K. Ronson, A. B. League, L. Gagliardi, C. J. Cramer and J. R. Nitschke, *J. Am. Chem. Soc.*, 2014, **136**, 15615–15624.
10 (*a*) C. Garcia-Simon, M. Garcia-Borras, L. Gomez, T. Parella, S. Osuna, J. Juanhuix, I. Imaz, D. Maspoch, M. Costas and X. Ribas, *Nat. Commun.*, 2014, **5**, 5557; (*b*) Y. Inokuma, T. Arai and M. Fujita, *Nat. Chem.*, 2010, **2**, 780–783.
11 S. Brooker, *Chem. Soc. Rev.*, 2015, **44**, 2880–2892.
12 T. K. Ronson, W. Meng and J. R. Nitschke, *J. Am. Chem. Soc.*, 2017, **139**, 9698–9707.
13 T. K. Ronson, B. S. Pilgrim and J. R. Nitschke, *J. Am. Chem. Soc.*, 2016, **138**, 10417–10420.
14 K. Rissanen, *Chem. Soc. Rev.*, 2017, **46**, 2638–2648.
15 S. Mecozzi and J. Rebek, *Chem. – Eur. J.*, 1998, **4**, 1016–1022.
16 R. A. Bilbeisi, S. Zarra, H. L. Feltham, G. N. Jameson, J. K. Clegg, S. Brooker and J. R. Nitschke, *Chem. – Eur. J.*, 2013, **19**, 8058–8062.
17 (*a*) D. Mihailovic, D. Arcon, P. Venturini, R. Blinc, A. Omerzu and P. Cevc, *Science*, 1995, **268**, 400–402; (*b*) K. Tanaka, T. Sato, K. Yoshizawa, K. Okahara, T. Yamabe and M. Tokumoto, *Chem. Phys. Lett.*, 1995, **237**, 123–126.